Self-pulsations and excitability in optically injected quantum-dot lasers: Impact of the excited states and spontaneous emission noise

Lukasz Olejniczak,[1,2,*] Krassimir Panajotov,[1,3] Hugo Thienpont,[1] and Marc Sciamanna[2]

[1]*Department of Applied Physics and Photonics, Brussels Photonics Team B-PHOT, Vrije Universiteit Brussel, 2 Pleinlaan, B-1050 Brussels, Belgium*

[2]*SUPELEC, OPTEL, & LMOPS EA 4423 (Laboratoire Matériaux Optiques, Photonique et Systèmes), 2 rue Edouard Belin, F-57070 Metz, France*

[3]*Institute of Solid State Physics, 72 Tzarigradsko Chaussee Boulevard, 1784 Sofia, Bulgaria*

(Received 29 March 2010; published 17 August 2010)

We study the dynamics of an optically injected quantum-dot laser accounting for excited states. Mapping of the bifurcations in the plane frequency detuning vs. injection strength shows that the relaxation rate scales the regions of locking and single- and double-period solutions, while the capture rate has a minor effect. Within the regions of time-periodic solutions, close to the saddle-node bifurcation boundary, we identify subregions where the output signal resembles excitable pulses as a result of the bottleneck phenomenon. We show that such emission is determined mainly by fluctuations in the occupation of the excited states. The interpulse time follows an inverse square root scaling law as a function of the detuning. In a deterministic system the pulses are periodic regardless of the detuning, but in the presence of noise, close to the locking region, the interpulse time follows a positively skewed normal distribution. For a fixed frequency detuning, increasing the noise strength can shift the mean of the interpulse time distribution and make the pulsations more periodic.

DOI: 10.1103/PhysRevA.82.023807 PACS number(s): 42.65.Sf, 42.55.Px, 05.45.−a

I. INTRODUCTION

Optical injection in quantum-well (QW) semiconductor lasers has been shown to be an attractive configuration for the fundamental bifurcation study of nonlinear optical systems [1–3] and provides a potential means of improving laser performance [4–6]. Recent experimental studies on optically injected quantum-dot (QD) lasers have revealed the existence of regions in the parameter space (defined by the frequency detuning from the slave laser frequency and the injection strength) where the laser responds to the injected optical signal in a form of single or double excitable pulses [7]. A system is excitable if, for a sufficiently strong perturbation, it can leave its rest state and fire a spike associated with a large excursion of the system's variables in the phase space [8]. Excitable pulses at positive detuning [7] and at both positive and negative detuning [9] have been observed. Excitability is not limited to optically injected QD lasers and such dynamics have already been reported for a variety of laser systems including lasers with optical feedback [10,11] and lasers with a saturable absorber [12]. In optically injected QW lasers excitable dynamics have been predicted theoretically [13,14] and very recently observed experimentally [15]. Detailed experimental study on the dynamics of excitable pulses in optically injected QD laser shows that they are dependent on the detuning so that the pulses become more frequent and more periodic as the detuning increases [9].

One of the features that distinguishes QD lasers from their QW counterparts is a more complicated dynamics of carriers, which, being captured from the wetting layer into the dots, achieve lasing states by successive transitions through excited states. This process is characterized by the capture and the relaxation times, respectively. Both time constants have been shown to influence the performance of QD lasers in terms of modulation bandwidth and threshold current [16–18]. An important question, which has not yet been investigated, concerns the impact of the two time constants on the dynamics of optically injected QD lasers. To answer this question we extend the model presented in [7] to account for the excited states and map the bifurcations of the system dynamics in the plane detuning vs. injection strength. Within the regions of time-periodic solutions we identify subregions of self-pulsations, where the laser deterministically, that is, without the addition of perturbation or noise, fires a time-periodic sequence of pulses resembling excitable ones. Such regions appear for both positive and negative detuning. We show that these self-pulsations are associated with the so-called bottleneck phenomenon [19]. We identify the role of the excited states in the emission of self-pulsations. We further study the dynamics of self-pulsations in the presence of spontaneous emission noise to compare it with the dynamics experimentally reported for excitable pulses [9]. In particular, we investigate how the interpulse time distribution changes as a function of the detuning and the noise strength.

The structure of the paper is as follows. In Sec. II we describe the theoretical model that we use in our calculations. In Sec. III we present the results on the influence of the relaxation and capture rates on the dynamics of optically injected QD lasers. In Sec. IV we focus on deterministic self-pulsations and then investigate their dynamics in the presence of spontaneous emission noise in Sec. V.

II. THEORETICAL MODEL

To account for the excited states of QDs we extended the theoretical model presented in [7]. In our approach, carriers from the wetting layer are first being captured into the excited state and then relax to the ground state [17]. The complete set

*olejniczak.lukasz@gmail.com

of equations reads:

$$\frac{dE}{dt} = \frac{1}{2}v_g g_0\left(2f_{GS} - 1 - \frac{\gamma_s}{v_g g_0}\right)(1+i\alpha)E + i\Delta E + \gamma_s\sqrt{\frac{S_m}{\hbar\omega}} + E_{noise}, \quad (1)$$

$$\frac{df_{WL}}{dt} = \frac{I}{q} - \gamma_n f_{WL} - \frac{f_{WL}(1-f_{ES})}{t_c}, \quad (2)$$

$$\frac{df_{ES}}{dt} = -\gamma_n f_{ES} + \frac{f_{WL}(1-f_{ES})}{4t_c} - \frac{f_{ES}(1-f_{GS})}{t_o}, \quad (3)$$

$$\frac{df_{GS}}{dt} = -\gamma_n f_{GS} + \frac{2f_{ES}(1-f_{GS})}{t_o} - v_g\sigma(2f_{GS}-1)|E|^2. \quad (4)$$

Here f_{WL}, f_{ES}, and f_{GS} describe the occupation probabilities, that is, the number of carriers in the wetting layer, excited state, and ground state, respectively, normalized to the product of the number of QDs and the degeneracy of the respective states. $|E|^2$ represents the intensity. The model contains four main time constants, namely, the carrier decay rate $\gamma_n = 1\ \mathrm{ns}^{-1}$, the photon decay rate $\gamma_s = 590\ \mathrm{ns}^{-1}$, the capture time t_c, and the relaxation time t_o. The linewidth enhancement factor is $\alpha = 1.2$, the linear optical gain coefficient is $g_0 = 72\ \mathrm{cm}^{-1}$, and the interaction cross section is $\sigma = 0.6\ \mathrm{nm}^2$. The pump current I is normalized to the number of QDs. The frequency of the master laser amounts to $\omega = 1.45 \times 10^{15}\ \mathrm{s}^{-1}$. The remaining parameters represent the group velocity $v_g = 0.833 \times 10^8$ m/s, the electric charge q, and the Planck constant $\hbar$. The frequency detuning Δ (the difference between the slave and the master laser frequency) and the energy density of the field injected from the master laser S_m define the parameter space. $E_{noise} = \sqrt{2\beta_{sp}\gamma_n f_{GS} N_{QD}}\varsigma$ constitutes the spontaneous emission noise term, in which ς is a white noise of unitary variance and 0 mean value, while N_{QD} is the volume density of QDs. The strength of the noise term is driven by the spontaneous recombination factor β_{sp}.

We have rewritten Eqs. (1)–(4) in a dimensionless form using the following variables: $F = E\sqrt{\frac{v_g\sigma}{\gamma_n}}$ as the normalized field, $a = \frac{1}{2}\frac{v_g g_0}{\gamma_n}$ as the normalized gain, $\gamma = \frac{\gamma_s}{v_g g_0}$ as the normalized photon decay rate, $J_n = \frac{I}{q\gamma_n}$ as the normalized pump current, $C = \frac{1}{t_c\gamma_n}$ as the normalized capture rate, $R = \frac{1}{t_o\gamma_n}$ as the normalized relaxation rate, and $B = \gamma_s\sqrt{\frac{v_g\sigma}{\hbar\omega\gamma_n^3}}$, $t_1 = t\gamma_n$, as the normalized time. The resulting equations are as follows:

$$\frac{dF}{dt_1} = a(2f_{GS} - 1 - \gamma)(1+i\alpha)F + i\frac{\Delta}{\gamma_n}F + B\sqrt{S_m} + F_{noise}, \quad (5)$$

$$\frac{df_{WL}}{dt_1} = J_n - f_{WL} - Cf_{WL}(1-f_{ES}), \quad (6)$$

$$\frac{df_{ES}}{dt_1} = -f_{ES} + \frac{Cf_{WL}(1-f_{ES})}{4} - Rf_{ES}(1-f_{GS}), \quad (7)$$

$$\frac{df_{GS}}{dt_1} = -f_{GS} + 2Rf_{ES}(1-f_{GS}) - (2f_{GS}-1)|F|^2. \quad (8)$$

In our calculations the normalized pump current is fixed at $J_n = 6.25$.

III. INFLUENCE OF THE RELAXATION AND CAPTURE TIMES ON THE DYNAMICS OF THE OPTICALLY INJECTED QUANTUM-DOT LASER

We first investigate the influence of the two main time constants that determine the QD laser dynamics, namely, the capture and relaxation times. To this aim we use the continuation and bifurcation software AUTO-07P [20]. The results for the relaxation rate are presented in Fig. 1. All three bifurcation maps contain a saddle-node (SN) bifurcation curve, a Hopf bifurcation (HB) curve, a homoclinic (HOM) bifurcation curve, a period-doubling (PD) bifurcation curve, and a curve corresponding to a SN bifurcation of limit cycles (LPC). The locking region is bordered by parts of the SN bifurcation and HB curves for a negative detuning and a branch of the SN bifurcation curve that verges with the region of a limit cycle (LC) for a positive detuning.

Comparing the bifurcation maps one can conclude that the relaxation rate strongly influences the size of regions of solutions emerging from the respective bifurcations. When the transitions from the excited states to the ground states are fast enough, our model recovers the results presented in [7]. A lower relaxation rate results in a broader locking region and shifts the position of point G_1, where the SN and HB curves are tangent, to a lower injection strength. It is demonstrated in the next section that the laser behavior for negative detuning outside the locking region is different on both sides of point G_1. The capture time turns out not to influence the dynamics of the system in the investigated range, that is, 1–10 ps.

In Fig. 1(a) the HOM bifurcation overlaps with parts of the SN bifurcation curve that border the locking region. However, at certain values of the injection strength, the HOM curve leaves the SN curve and forms the so-called homoclinic tooth (HOM), which penetrates into the locking region. It has been shown in [14,21] and [22] that HOM bifurcation is associated with self-pulsations and excitability and constitutes a boundary between these two dynamics. As a result, close to the HOM curve, before the onset of self-pulsations, the laser is excitable; that is, sufficiently strong perturbation can force the system to fire pulses. Excitability in close proximity to the HOM tooth is associated with the SN HOM orbit bifurcation [21]. It has been shown in [7] that optically injected QD lasers can fire single or double excitable pulses, the latter being related to a nearby PD. Examples of triggered single and double excitable pulses are shown in Figs. 2(a) and 2(b). We triggered the laser by suddenly changing its variables (the duration of such perturbation is 0.1 ns) so that the laser is kicked out from the attractor corresponding to a locked state and makes a quick excursion along the unstable manifold of the saddle [13] back to the attractor. Both fixed points emerge from a nearby SN bifurcation. Inside the HOM tooth the laser either can be locked or can exhibit self-pulsations associated with the attracting LC. An unperturbed laser remains in the locked state and, therefore, to observe self-pulsations inside the HOM tooth, the system needs to be kicked out of the attractor corresponding to the locked state to the vicinity of attraction of the LC. Such bistable behavior is presented in Fig. 2(c).

As shown in Figs. 1(b) and 1(c), at lower relaxation rates additional teeth arise and mostly fill the region bordered by the

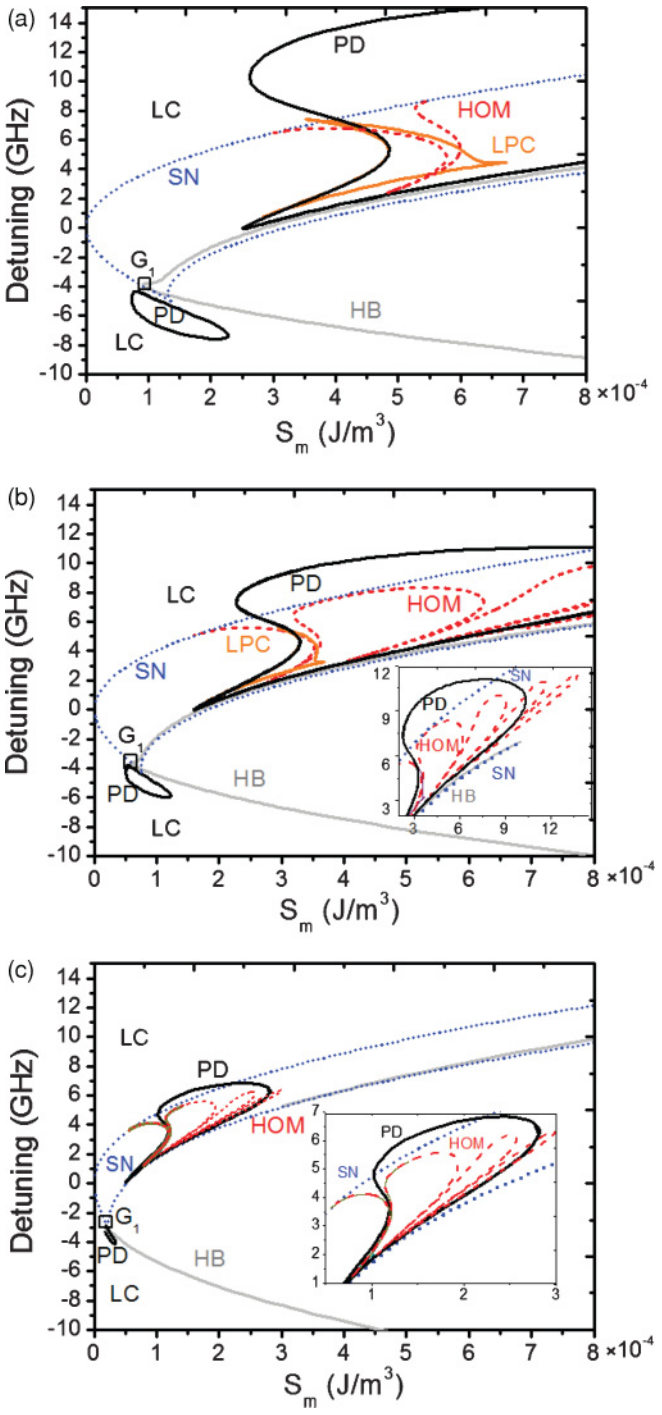

FIG. 1. (Color online) Bifurcation map of equilibria and limit cycles (LCs) when the normalized relaxation rate R is equal to (a) 1020, (b) 500, and (c) 200. The normalized current amounts to $J_n = 6.25$. Solid, light-gray curve (HB), Hopf bifurcation; dotted gray (blue) curve (SN), saddle-node bifurcation; solid black curve (PD), period-doubling bifurcation; dashed gray (red) curve (HOM), homoclinic bifurcation; solid gray (orange) curve (LPC), saddle-node bifurcation of LCs. G_1: saddle-node Hopf bifurcation point.

PD bifurcation curve. Contrary to the main HOM tooth, the consecutive HOM teeth are not tangent to the SN bifurcation curve. Detailed study of this issue is outside the scope of this paper.

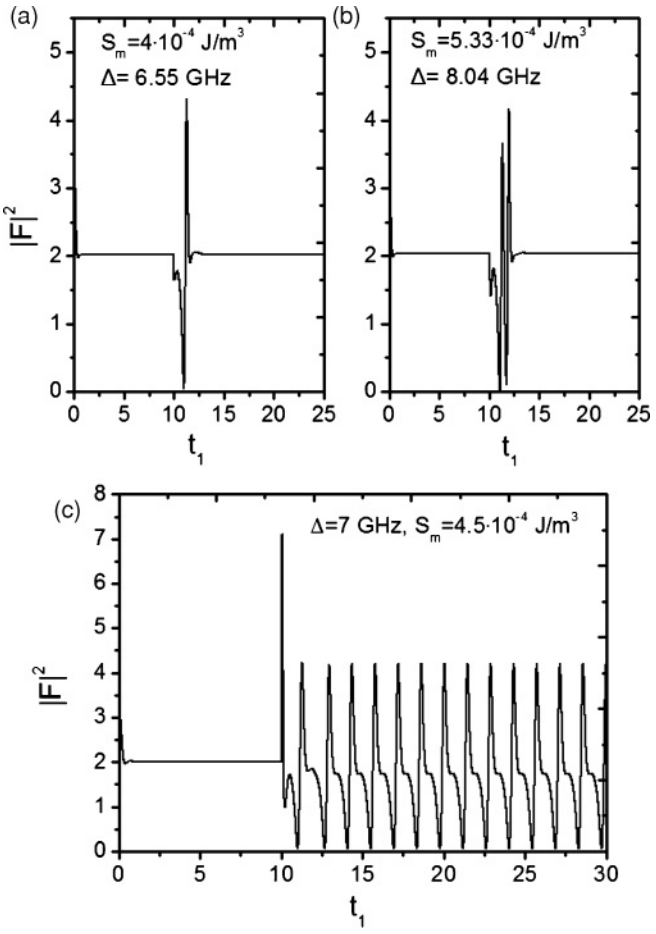

FIG. 2. Examples of triggered (a) single-pulse excitability ($\Delta = 6.55$ GHz, $S_m = 4 \times 10^{-4}$ J/m^3) and (b) double-pulse excitability ($\Delta = 8.04$ GHz, $S_m = 5.33 \times 10^{-4}$ J/m^3). (c) Bistability between the attractor corresponding to the locked state and the attracting limit cycle associated with self-pulsations inside the homoclinic tooth: $S_m = 4.5 \times 10^{-4}$ J/m^3, $\Delta = 7.0$ GHz.

The slave laser is also excitable away from the HOM tooth, in close proximity to parts of the SN curve that overlap with the HOM curve. Excitability there is related to a SN-on-LC bifurcation [21]. As such parts exist for both positive and negative detuning, the laser can exhibit this type of excitability on both sides of the locking region. This has been shown experimentally in [9]. Because the HOM constitutes a boundary between excitability and self-pulsations, one can expect that outside the locking region, close to the SN bifurcation curve, the slave laser will exhibit self-pulsations. We investigate this issue in Sec. IV.

IV. SELF-PULSATIONS DUE TO THE BOTTLENECK PHENOMENON

So far we have analyzed bifurcation maps computed with AUTO. This software allows us to continue steady and time-periodic solutions of a dynamical system and to detect their stability changes and, therefore, bifurcations. An alternative approach for detecting bifurcations is to analyze intensity time traces obtained from direct numerical integration for different values of a bifurcation parameter. Therefore, to calculate

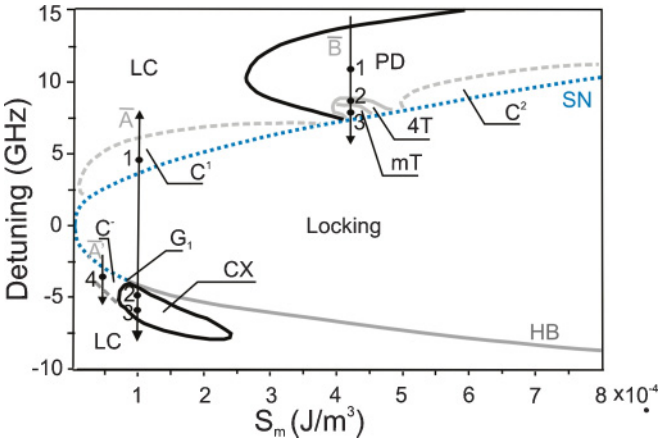

FIG. 3. (Color online) Map of bifurcations for an optically injected quantum-dot laser obtained by analyzing time traces of $|F|^2$ for a relaxation rate $R = 1020$. Inside LC the laser exhibits period 1 time-periodic oscillations associated with the limit cycle; inside the period-doubling (PD) bifurcation, period 2 time-periodic oscillations. C^1 and C^- correspond to single-pulse self-pulsations for positive and negative detuning, respectively; C^2 corresponds to double-pulse self-pulsations; 4T corresponds to period 4 time-periodic oscillations; mT corresponds to chaotic oscillations. Region CX corresponds to a set of injection parameters bordered by the PD bifurcation curve in Fig. 1(a). Inside this region the slave laser exhibits quite diversified dynamics including period 1 and period 2 time-periodic and chaotic oscillations. Dotted gray (blue) line (SN), saddle-node bifurcation; solid light-gray curve (HB), Hopf bifurcation. G_1: saddle-node Hopf bifurcation point.

complete bifurcation maps such as those presented in Fig. 1, one needs to run many computations starting at different points in the (Δ, S_m) plane. We use this method to analyze the behavior of the slave laser outside the locking region but in close proximity to branches of the SN curve that border the locking region. The resulting map is presented in Fig. 3 [the parameters are consistent with those used to calculate the bifurcation map presented in Fig. 1(a)]. It should be stressed here that this bifurcation map accounts only for stable solutions. Similarly to Fig. 1(a), we can distinguish regions of time-periodic solutions (LC), double-period solutions (PD), and locking. The new information brought by Fig. 3 is the presence of regions C^-, C^1, C^2, 4T, mT, and CX. The first three regions correspond to deterministic single-pulse (C^-, C^1) and double-pulse (C^2) self-pulsations. They are not associated with a new bifurcation but with a change of the waveform, and to highlight the difference they are bordered by gray dashed curves in Fig. 3. Regions 4T and mT correspond to period 4 time-periodic and chaotic oscillations, respectively. Region CX corresponds to a set of injection parameters bordered by the PD bifurcation curve in Fig. 1(a). As shown later, inside this region the slave laser exhibits quite diversified dynamics including period 1 and period 2 time-periodic and chaotic oscillations. To characterize all the new regions we compute the bifurcation diagrams showing different extrema (maxima and minima) in the time traces of $|F|^2$ as a function of the detuning. A bifurcation diagram crossing the regions C^1, CX, and C^- along arrow $\bar{A}$ and the corresponding time traces are presented in Figs. 4(a) and 4(b), respectively. The top

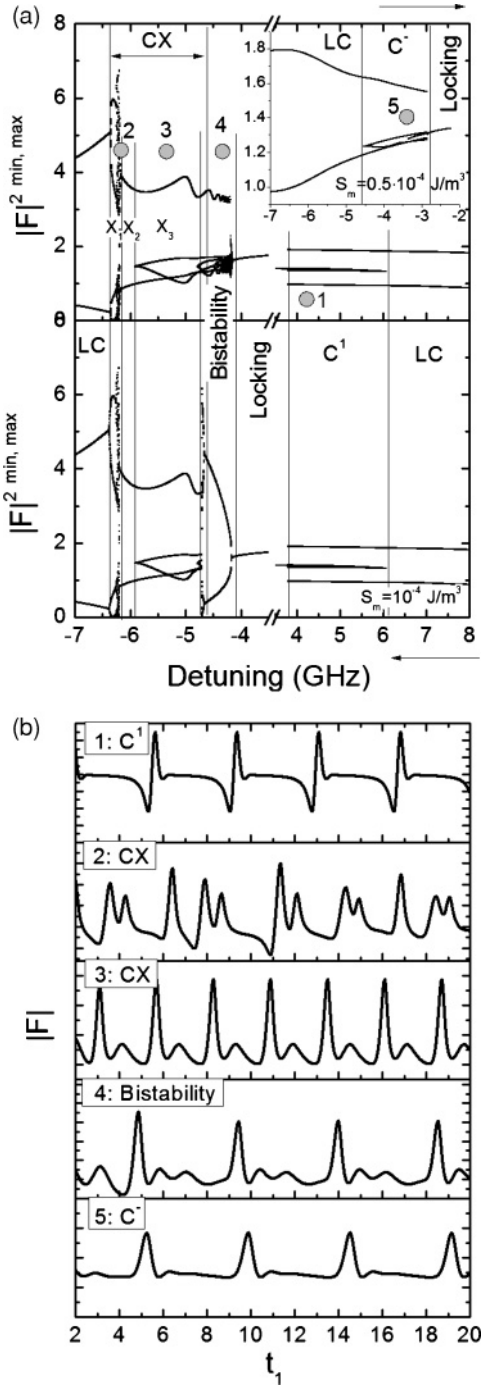

FIG. 4. (a) Bifurcation diagram for $S_m = 10^{-4}$ J/m^3 (inset: bifurcation diagram for $S_m = 0.5 \times 10^{-4}$ J/m^3) when sweeping the detuning either from negative to positive (top) or from positive to negative (bottom) values. (b) Examples of time traces along arrows A and A′ in Fig. 3: (1) $\Delta = 4.2$ GHz; (2) $\Delta = -6.177$ GHz; (3) $\Delta = -5.5$ GHz; (4) $\Delta = -4.5$ GHz; (5) $\Delta = -3.2$ GHz.

plot in Fig. 4(a) corresponds to the sweeping of the detuning from negative toward positive values, whereas the bottom plot corresponds to the opposite direction of sweeping.

We first describe the bifurcation diagram for positive detuning. As can be concluded from a comparison between the top and the bottom plots in Fig. 4(a), it is indifferent

to the sweeping direction. At a large value of detuning the laser exhibits period 1 time-periodic oscillations (LC). When the detuning decreases, in region C^1 the waveform of these periodic oscillations changes [see the time trace in Fig. 4(b)–1, corresponding to gray circle 1 in the top plot in Fig. 4(a)] so that it resembles single excitable pulses in Fig. 2(a). Inside C^1 the algorithm used to analyze time traces of $|F|^2$ detects two additional local extrema between those corresponding to an unbroken limit cycle associated with periodic oscillations in LC [both plots in Fig. 4(a)]. These additional extrema correspond to strongly damped, low-amplitude oscillations that follow the main spike [see Fig. 4(b)–1]. Below C^1, close to the SN curve, the laser can fire excitable pulses related to a SN-on-LC bifurcation. We, therefore, classify solutions in C^1 as deterministic single-pulse self-pulsations.

For negative detuning the bifurcation diagram reveals a strong dependence on the sweeping direction. In addition, Fig. 3 shows that the behavior of the slave laser for negative detuning should vary on different sides of the point G_1. On its high-injection-strength side the locking region is bordered by the HB curve. In the top plot in Fig. 4(a), when the HB curve is approached from a large, negative value of detuning, the laser first exhibits period 1 time-periodic oscillations (LC) and then enters the region CX. To describe its behavior inside CX, we divided this region into subregions X_1–X_3. Inside X_1 the waveform of periodic oscillations from LC undergoes a PD cascade to chaos [see Fig. 4(b)–2 for the chaotic time trace corresponding to gray circle 2 in the top plot in Fig. 4(a)]. Consecutively, in the narrow range of the detuning corresponding to X_2, the laser again exhibits period 1 time-periodic oscillations and then, in subregion X_3, period 2 time-periodic oscillations as in Fig. 4(b)–3. At still smaller detuning, close to the boundary of CX, there is a region of bistability [see Fig. 4(a)]. In this region, when sweeping the detuning from negative toward positive values, the system fires pulses followed by damped, low-amplitude oscillation as in Fig. 4(b)–4. This shows that the dynamics of the system is influenced by the SN bifurcation. Indeed, as shown in Fig. 1(a), the SN curve first crosses the HB curve at point G_1 and then it enters the unlocked region. The region of bistability, therefore, extends to the injection strength reached by the SN curve in the unlocked region. The alternative solution in the region of bistability corresponds to period 1 time-periodic oscillations (not shown). Such behavior is possible when the detuning changes from positive toward negative values. On the low-injection-strength side of point G_1, the locking region is bordered by the SN bifurcation. The bifurcation diagram along arrow $\bar{A}'$ in Fig. 3 is shown in the inset in the top plot in Fig. 4(a). Inside C^- the laser fires pulses as demonstrated in Fig. 4(b)–5. We consider these pulses to be deterministic self-pulsations for negative detuning.

A bifurcation diagram along arrow $\bar{B}$ in Fig. 3 is presented in Fig. 5(a). The limit cycle first undergoes PD bifurcation [see also the time trace in Fig. 5(b)–1] and then enters regions 4T and mT of period 4 time-periodic and chaotic oscillations, respectively [see time traces in Figs. 5(b)–2 and 5(b)–3].

In region C^2 the laser exhibits double-pulse self-pulsations (see also the time trace for the amplitude of the electric field in Fig. 7) resembling the double-pulse excitability in Fig. 2(b).

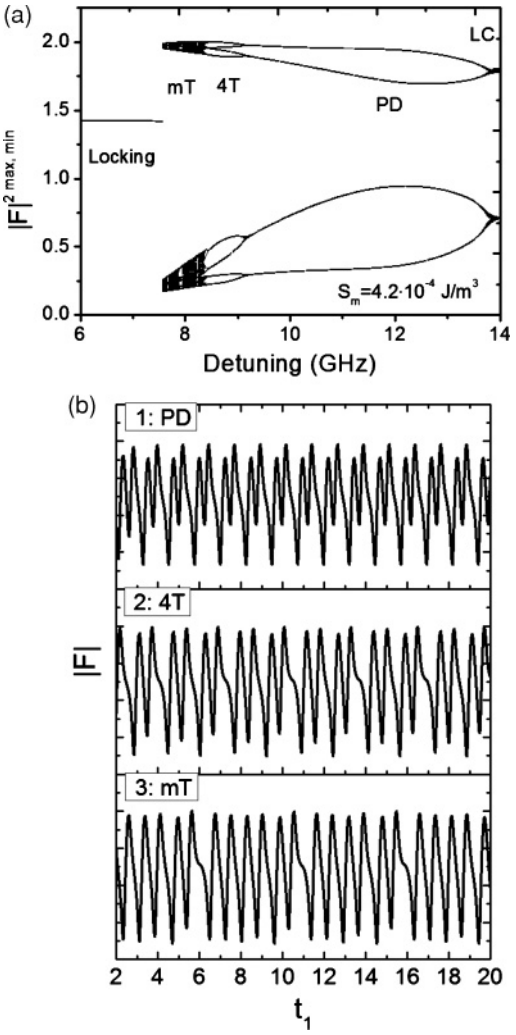

FIG. 5. (a) Bifurcation diagram for $S_m = 4.2 \times 10^{-4}$ J/m^3. (b) Examples of time traces along arrow B in Fig. 3: (1) $\Delta =$ 11.0 GHz; (2) $\Delta = 8.8$ GHz; (3) $\Delta = 8.0$ GHz.

We would like to stress that the self-pulsations in regions $C^{1,2,-}$ are observed deterministically, without the need for an additional perturbation, unlike the self-pulsations that appear inside the HOM tooth (and shown in Fig. 2(c)). These self-pulsations result from the so-called bottleneck [19]. In this mechanism, after the SN bifurcation a saddle remnant (or "ghost") can continue influencing the system, although the two fixed points involved in the bifurcation annihilate. In Fig. 6(a) we show the phase diagrams corresponding to the regions below C^1 and inside of C^1 (coordinates of the fixed points have been calculated by DSTOOL [23]). Indeed, inside C^1 the shape of the attractor is influenced by the "ghost" of a saddle. In Fig. 6(b) we show the time difference between consecutive pulses in region C^1 as a function of the detuning. It follows an inverse square root law that is characteristic of the bottleneck phenomenon [24]. In the deterministic system [the noise term in Eq. (1) is neglected], the pulses are periodic regardless of the detuning. The repetition rate on the edge between C^1 and LC is of 0.5 GHz. The same behavior can be observed in regions C^- and C^2. We would like to mention that the repetition rate of

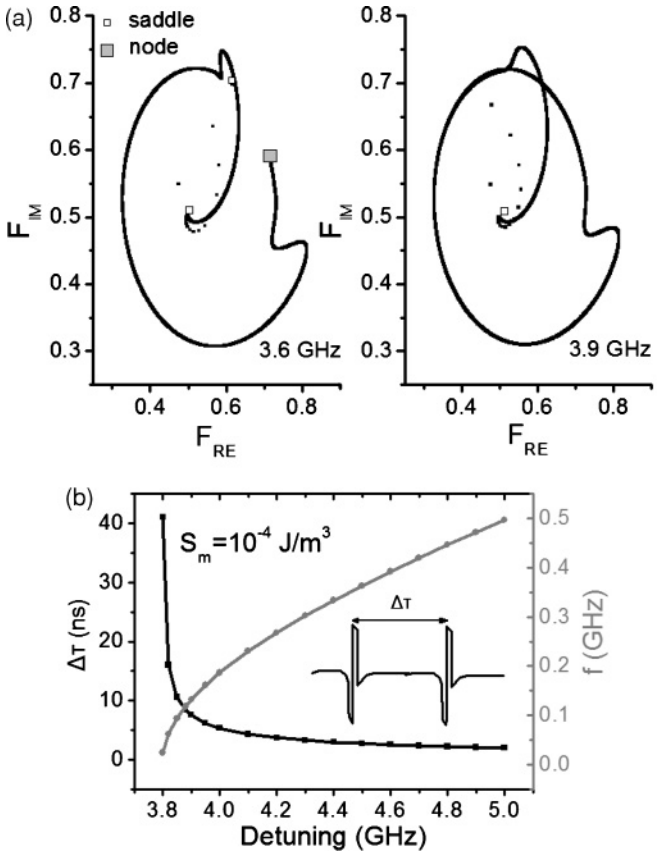

FIG. 6. (a) Phase diagram for $S_m = 10^{-4}$ J/m^3 and (left) $\Delta = 3.6$ GHz and (right) $\Delta = 3.9$ GHz. (b) Time difference (and corresponding frequency, f) between consecutive pulses in region C^1 as a function of the detuning.

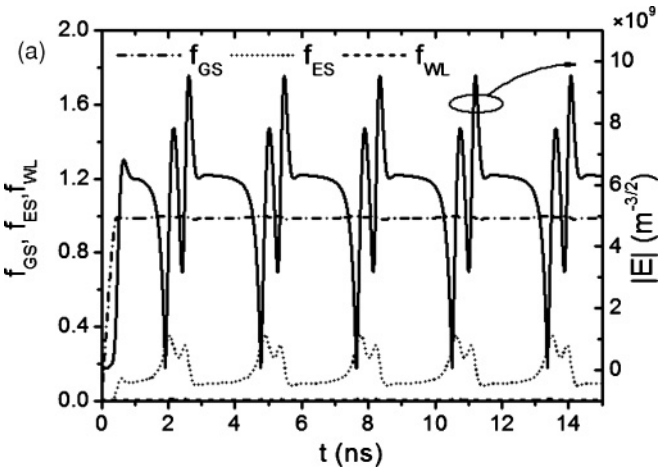

FIG. 7. Temporal changes in the occupation probabilities of the respective energy levels when the laser exhibits double-pulse self-pulsations. $\Delta = 9.4$ GHz, $S_m = 6 \times 10^{-4}$ J/m^3.

experimentally observed excitable pulses also increases when the detuning is increased [9].

An important question here is how the QD excited state contributes to the emission of self-pulsations. Temporal changes in the occupation of the respective energy levels for a laser exhibiting double-pulse self-pulsations (C^2) are shown in Fig. 7. With the parameter setting used in the model, the ground state, which is represented by the dot-dashed curve, is saturated. The excited state, represented by the dotted line, is far from saturation and it seems that the shape of the emitted signal is determined mainly by moderate changes in the occupation of this state. Its fluctuations influence the occupation of the ground state through the Pauli blocking term in the expression of the relaxation term. However, the amplitude of these oscillations is much lower than it is the case for the excited level.

V. EFFECT OF SPONTANEOUS EMISSION NOISE ON THE DYNAMICS OF SELF-PULSATIONS

Excitable pulses can exist only if a perturbation is present in the system, for example, noise, so that the excitability threshold can be overcome. As characterized in Sec. IV, self-pulsations are, however, possible in the absence of noise and they resemble the excitable pulses in Figs. 2(a) and 2(b). In experiments noise is inherent to the lasing emission and it is therefore difficult to distinguish between excitability and self-pulsation by looking only at the intensity waveforms. To make our analysis complete, in this section we show that the self-pulsations, when accounting for spontaneous emission noise in the model, moreover, have statistical characteristics similar to those observed experimentally for the excitable pulses [9].

Examples of time traces for different values of the detuning in the presence of noise are shown in Fig. 8. Compared to the case without noise, the time between consecutive pulses for a fixed value of the detuning is no longer constant. Nevertheless, the repetition rate still increases with the detuning. Interpulse time distributions for two values of the detuning corresponding to the edge between locking and C^1, and between C^1 and LC, are presented in the inset in Fig. 8. In the former case (black distribution) the interpulse time follows a positively skewed normal distribution. In the latter case (gray distribution) the distribution is sharp, while its mean is shifted toward smaller values. This behavior is consistent with that reported in [9] in the regions considered to be excitable.

The interpulse time distribution for double-pulse self-pulsations is shown in Fig. 9. Two, well-resolved peaks correspond to the time between consecutive double-pulse self-pulsations and to the time between spikes within a single double-pulse self-pulsation. Analyzing the number of peaks of such a distribution has been proposed as a way to detect and distinguish different types of multipulse excitabilities in an experiment [13]. It can be concluded from the inset in Fig. 9 that the noise can break the regularity of self-pulsations as, for example, in the time slot between 492 and 495 ns, where a double pulse is lost at the expense of more periodic oscillations.

In Fig. 10 the influence of spontaneous emission noise on the standard deviation σ [Fig. 10(a)] and the mean $\langle T \rangle$ [Fig. 10(b)] of the interpulse time distribution for different values of the detuning is presented. For a detuning of 3.8 GHz, which is at the SN bifurcation curve bordering the locking region for positive detuning, the noise influences both σ and

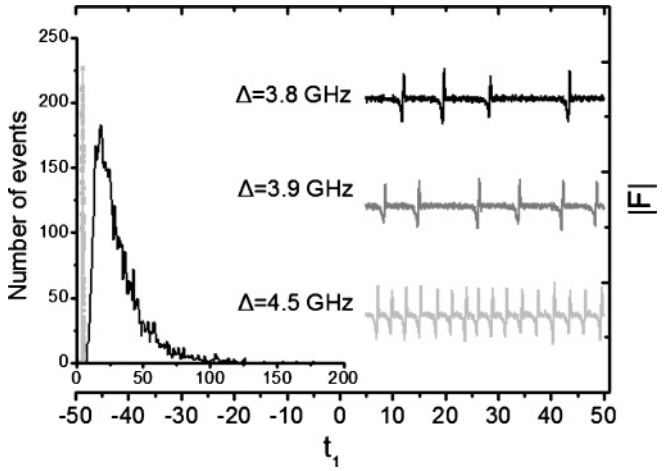

FIG. 8. Time traces for different values of the detuning in the presence of spontaneous emission noise, $S_m = 10^{-4}$ J/m^3. Inset: Distribution of the interpulse time for detunings of 3.8 GHz (black curve) and 4.5 GHz (gray curve).

$\langle T \rangle$. Although, for a very small noise, when $\beta_{sp} < 10^{-8}$, the pulses are periodic [see also the time trace in Fig. 10(c)–1], this periodicity is rapidly broken at a slightly larger noise value. At $\beta_{sp} = 10^{-7}$, σ achieves its maximum and then decreases with increasing noise. The mean of the distribution decreases monotonously with increasing noise—after, however, a sharp decrease for $\beta_{sp} < 10^{-6}$. Such behavior indicates that close to the locking region, the spontaneous emission noise influences the dynamics of self-pulsations in the same way as the detuning does for a fixed value of noise; that is, it shifts the mean toward smaller values and makes the pulsations more and more periodic [Figs. 10(c)–3 and 10(c)–4]. In contrast, for a detuning of 3.9 GHz the noise seems not to influence the mean. The standard deviation increases for $\beta_{sp} < 10^{-6}$ and then saturates. For $\beta_{sp} = 10^{-4}$ the output signal becomes very noisy so that both the mean and the standard deviation approach 0 [see Fig. 10(c)–5].

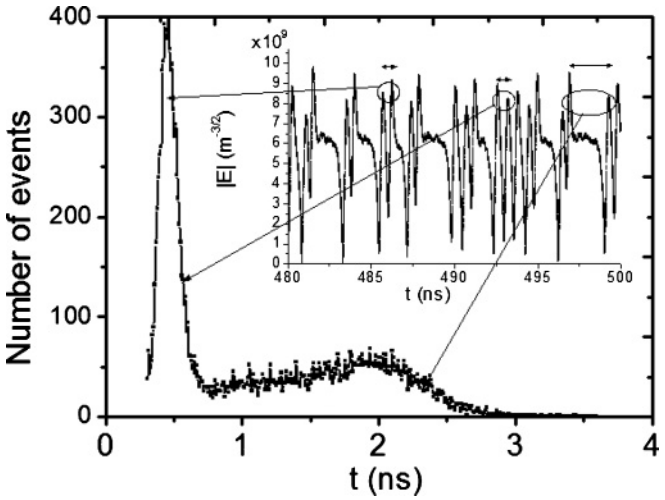

FIG. 9. Statistics of the interpulse time for double pulses. $\Delta = 9.6$ GHz, $S_m = 6 \times 10^{-4}$ J/m^3.

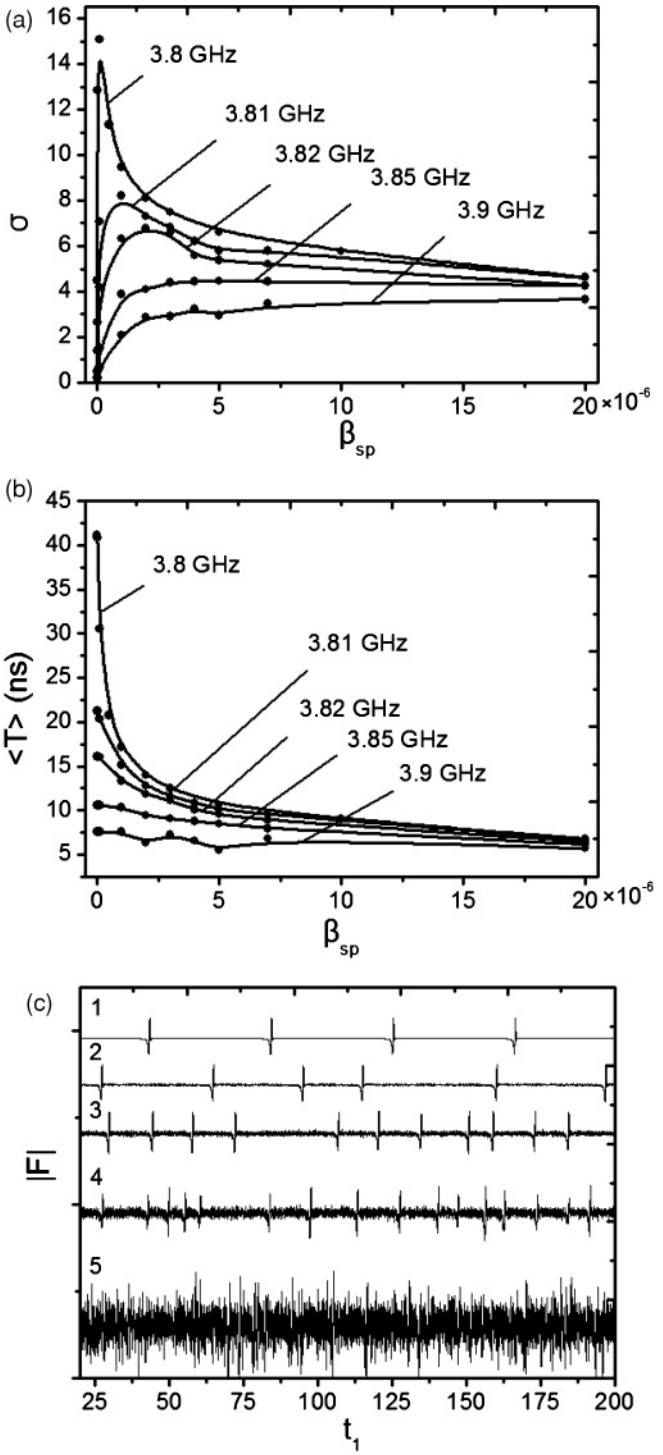

FIG. 10. (a) Standard deviation σ and (b) mean $\langle T \rangle$ of the interpulse time distribution as a function of the spontaneous recombination noise strength. $S_m = 10^{-4}$ J/m^3. (c) Examples of time traces at the detuning of 3.8 GHz and (1) $\beta_{sp} = 0$, (2) $\beta_{sp} = 10^{-7}$, (3) $\beta_{sp} = 10^{-6}$, (4) $\beta_{sp} = 5 \times 10^{-6}$, and (5) $\beta_{sp} = 10^{-4}$.

VI. CONCLUSIONS

We have expanded a theoretical model for optically injected QD lasers to account for the excited states and intradot transitions of carriers. The model allows us to check the influence of the main time constants, namely, the capture

and relaxation times. Our results show that the dynamics of optically injected QD lasers are determined mainly by the relaxation time. Among other things, it scales the regions of locking and single- and double-period solutions. The capture time has a minor impact on the dynamics. Bifurcation maps calculated with continuation and bifurcation software have been compared with the bifurcation map obtained by analysis of the intensity time traces. With the latter method, within the regions of periodic solutions we are able to identify subregions where the laser deterministically fires a time-periodic sequence of single or double pulses resembling excitable ones. These are C^1, C^2, and C^- in Fig. 3. We refer to these solutions as deterministic self-pulsations resulting from the bottleneck phenomenon [19,24]. Regions of single-pulse self-pulsations appear for both positive and negative detuning. Our results suggest that such emission is mainly determined by fluctuations in the occupation of excited states.

To make a complete comparison between the dynamics of self-pulsations and excitable pulses, we have accounted for the spontaneous emission noise in the model. The results presented in this paper refer mainly to self-pulsations existing inside C^1 but they hold for C^- and C^2 as well. In both deterministic and stochastic systems the interpulse time changes with the detuning according to an inverse square root scaling low. However, in a deterministic system the pulses are periodic regardless of the detuning, which is not the case in the presence of noise. In this case, close to the SN curve the interpulse time follows a positively skewed normal distribution. The distribution becomes sharp for higher values of the detuning when the unbroken LC is being approached. The behavior described is consistent with the experimental observations for excitable pulses [9].

Finally, we show that in the closest proximity to the SN curve, the noise strength influences the dynamics of self-pulsations in the same way as the detuning does when the noise is fixed. For larger values of detuning, in a given range of realistic spontaneous emission noise levels, the mean and the standard deviation saturate so that the dynamics of self-pulsations seems not to be affected by the noise. A noise-induced resonance of the time between pulses has not been observed when accounting only for spontaneous emission noise. Whether another external additive noise source (such as one added to the injection current) can bring the system to a coherence or stochastic resonance behavior [25,26] is an interesting question for future work.

ACKNOWLEDGMENTS

The authors acknowledge the financial support of Conseil Regional de Lorraine, BELSPO IAP 6/10, FWO-Vlaanderen, OZR-VUB for the GOA and IOF Projects, and COST MP0702.

[1] R. Lang, IEEE J. Quantum Electron. **18**, 976 (1982).
[2] S. Wieczorek, B. Krauskopf, T. B. Simpson, and D. Lenstra, Phys. Rep. **416**, 1 (2005).
[3] M. Sciamanna and K. Panajotov, Phys. Rev. A **73**, 023811 (2006).
[4] T. B. Simpson, J. M. Liu, and A. Gavrielides, IEEE J. Quantum Electron. **32**, 1456 (1996).
[5] T. B. Simpson, J. M. Liu, and A. Gavrielides, IEEE Photonics Technol. Lett. **7**, 709 (1995).
[6] E. K. Lau, L. J. Wong, X. Zhao, Y.-K. Chen, C. J. Chang-Hasnain, and M. C. Wu, J. Lightwave Technol. **26**, 2584 (2008).
[7] D. Goulding, S. P. Hegarty, O. Rasskazov, S. Melnik, M. Hartnett, G. Greene, J. G. McInerney, D. Rachinskii, and G. Huyet, Phys. Rev. Lett. **98**, 153903 (2007).
[8] B. Lindnera, J. Garcia-Ojalvo, A. Neimand, and L. Schimansky-Geier, Phys. Rep. **392**, 321 (2004).
[9] B. Kelleher *et al.*, Opt. Lett. **34**, 440 (2009).
[10] M. C. Eguia and G. B. Mindlin, Phys. Rev. E **60**, 1551 (1999).
[11] A. M. Yacomotti, M. C. Eguia, J. Aliaga, O. E. Martinez, G. B. Mindlin, and A. Lipsich, Phys. Rev. Lett. **83**, 292 (1999).
[12] J. L. A. Dubbeldam, B. Krauskopf, and D. Lenstra, Phys. Rev. E **60**, 6580 (1999).
[13] S. Wieczorek and D. Lenstra, Phys. Rev. E **69**, 016218 (2004).
[14] S. Wieczorek, B. Krauskopf, and D. Lenstra, Phys. Rev. Lett. **88**, 063901 (2002).
[15] O. Vaudel, N. Péraud, and P. Besnard, Proc. SPIE **6997**, 69970F (2008).
[16] C. Tong, D. Xu, and S. F. Yoon, J. Lightwave Technol. **27**, 5442 (2009).
[17] A. Markus, J. X. Chen, O. Gauthier-Lafaye, J.-G. Provost, C. Paranthoen, and A. Fiore, IEEE J. Sel. Top. Quantum Electron. **9**, 1308 (2003).
[18] V. V. Lysak, A. V. Shulika, and I. A. Sukhoivanov, in *Proceedings of International Workshop on Laser and Fiber-Optical Networks Modeling LFNM'01, Ukraine, 22–24 May, 2001* (Kharkiv, Ukraine, 2001), pp. 64–68.
[19] S. H. Strogatz, *Nonlinear Dynamics and Chaos: with Applications in Physics, Biology, Chemistry, and Engineering* (Westview Press, Boulder, CO, 1994).
[20] Available at [http://indy.cs.concordia.ca/auto/].
[21] S. Wieczorek and B. Krauskopf, Nonlinearity **18**, 1095 (2005).
[22] B. Krauskopf, K. Schneider, J. Sieber, S. Wieczorek, and M. Wolfrum, Opt. Commun. **215**(4–6), 367 (2003).
[23] Available at [http://mathlab.cit.cornell.edu/dyn_sys/dstool/dstool.html].
[24] E. Fontich and J. Sardanyes, J. Phys. A **41**, 015102 (2008).
[25] O. V. Ushakov, H.-J. Wuünsche, F. Henneberger, I. A. Khovanov, L. Schimansky-Geier, and M. Zaks, Phys. Rev. Lett. **95**, 123903 (2005).
[26] M. Arizaleta Arteaga, M. Valencia, M. Sciamanna, H. Thienpont, M. López-Amo, and K. Panajotov, Phys. Rev. Lett. **99**, 023903 (2007).